ARTICLES

van der Waals Broadening of the Electronic Spectra of 1-Azabicyclo[2.2.2]octane: Inversion into Lennard-Jones Pair Potentials

Arthur M. Halpern,* B. R. Ramachandran, and Ali Tagol†

Department of Chemistry, Indiana State University, Terre Haute, Indiana 47809

Received: October 28, 1997; In Final Form: December 30, 1997

Collisional perturbations of the $S_0 \rightarrow S_1$ and $S_0 \rightarrow S_2$ electronic transitions of 1-azabicyclo[2.2.2]octane (ABCO) by Ar, He, Xe, and SF_6 are studied under static-cell conditions at 296 K. Pressures ranged up to ca. 20 atm for Xe and SF_6 and ca. 80 atm for Ar and He. For all perturbers except for He, the vibronic features are red-shifted and broadened asymmetrically to the blue. For He a slight blue shift is observed. Linear shift coefficients for the 0−0 bands of these transitions are reported for the perturbers studied. The spectral perturbations caused by these agents are analyzed globally for each transition using an iterative Fourier reconvolution (IFR) method. Because of the distortion of the more weakly allowed $S_0 \rightarrow S_1$ transition by the $S_0 \rightarrow S_2$ transition, the IFR method was applied to the latter system using Lennard-Jones (LJ) pair potentials to model the interactions between the perturber and the S_0 and S_2 states of ABCO. In all cases good overall fits are achieved (χ^2 ca. 10^{-4}). For all perturbers, the LJ *R* values are larger for the S_2-perturber complex than for the ground state. For He and Ar, the excited-state well depth is smaller relative to the ground state; for SF_6 and Xe, the opposite is found. Results are compared with fluorescence lifetime and efficiency data of ABCO acquired at perturber pressures below 1 atm. The results of recent studies of ABCO−Ar in a supersonic beam are discussed in the context of the LJ potentials obtained in this study.

Introduction

It has long been recognized that extravalence or Rydberg transitions can be experimentally distinguished from their intravalence counterparts by their higher susceptibility to external perturbations, such as increased pressure[1] or electric field strength.[2] Thus, under the application of ca. tens of atm of an "inert" gas, such as Ar or He, the distinguishing vibronic features of a Rydberg transition become asymmetrically broadened and red (or blue)-shifted. In the limit of very high pressure, i.e., in the condensed phase, these vibronic features are often completely obliterated, and the spectrum becomes featureless and may manifest a Gaussian appearance in the absence of the interference of nearby transitions. Such transitions usually undergo blue shifts when the absorber is in the condensed phase.

Until recently, these pressure perturbation effects had been interpreted qualitatively in terms of the difference in the absorber−perturber interaction potentials for the absorber ground and electronically excited states.[1] We have developed a technique that quantitatively accounts for these pressure perturbations within the framework of centrosymmetric pair potentials, which are used to model the interactions between the perturber and the ground and the electronically excited absorber.[3,4] This method, which utilizes an iterative Fourier reconvolution procedure, allows one to invert the observed pressure-perturbed spectrum of an absorber into the ground- and excited-state interaction potentials vis-à-vis the perturber. This approach has been applied to several well-known molecular Rydberg spectra, such as the $\tilde{X} \rightarrow \tilde{B}$ transition in methyl iodide,[4] the $\tilde{X} \rightarrow \tilde{A}$ transition in ammonia,[5] and the $\tilde{X} \rightarrow \tilde{B}$ transition in acetone.[6]

We report here the employment of this method to the interpretation of the pressure-perturbed spectra of the saturated cage amine, 1-azabicyclo[2.2.2]octane (ABCO). Because of the structural rigidity of this compound, the low-frequency vibrational degrees of freedom and low-barrier internal rotations, which are responsible for the obscuration of vibrational detail in the room-temperature electronic spectra of acyclic trialkylamines, are nearly eliminated, and thus ABCO reveals considerable vibronic detail in its electronic spectra, even at room temperature.[7] These vibronically rich spectra are, in turn, amenable to pressure perturbation studies, which can be used to elucidate the interaction potentials of ABCO's ground and electronically excited states and the perturbing species. This system represents a particularly challenging application of the method both because the vibronic features of these electronic transitions are complex and congested and also because these low-lying transitions are relatively close to each other. Thus, we were interested in determining how well the method worked in a global analysis of the multimode set of progressions (and sequences) that makes up the ambient temperature absorption spectra of ABCO.

The low-lying electronic transitions of ABCO have been the focus of many experimental investigations involving both static cell[7] and jet-cooled conditions, including resonance-enhanced multiphoton ionization (REMPI),[8] two-photon fluorescence

† Present address: Ciba Specialty Chemicals Corporation, Tarrytown, NY 10591-9005.

S1089-5639(97)03470-1 CCC: $15.00
Published on Web 03/19/1998

excitation,[9] one-photon fluorescence excitation,[10] and recently mass-resolved excitation spectra (MRES).[11,12] In addition, there has been very recent interest in the characterization of the low-lying excited states of ABCO using ab initio computational methods.[13,14]

The interactions of a probe molecule such as ABCO with perturbers are relevant to the issue of solvation. Several years ago, we reported the results of a study in which the photophysical properties of ABCO, e.g., the radiative and nonradiative rate constants of the S_1 state (k_r and k_{nr}, respectively), were obtained as a function of perturber pressure (e.g., Ar and other rare gases).[15] We found that increases in both k_r and k_{nr} occurred at surprisingly low Ar pressures, i.e., on the order of tens of Torr; at higher pressures (but below 1 atm), these k_r and k_{nr} values leveled off, approaching the respective condensed phase (i.e., *n*-hexane) values.[15] Thus, it appears that "solvation", as it pertains to the effects on photophysical properties, is nearly complete at very low levels of solute interaction, possibly even on a 1:1 (pairwise) basis. The nonradiative consequences of 1:1 clustering of the excited state of ABCO with Ar in a supersonic jet have been recently discussed by Shang et al.[11,12] The present paper reports the effects of these perturbers on the $S_0 \rightarrow S_1$ and $S_0 \rightarrow S_2$ transitions at higher pressures of these gases.

The Method

The iterative Fourier reconvolution procedure that is used to invert the centrosymmetric pair potentials, ABCO−X and ABCO*−X (where X is the perturber and the asterisk denotes S_1 or S_2), from the pressure-pertubed spectra has been presented in detail previously.[4] We will outline the technique here briefly. The method relies on the dipole correlator approach[16] to the description of an electronic transition. The observed, unperturbed spectrum representing a single electronic transition is related to the complex function, $F(\tilde{\nu})$, which is expressed by the half-range Fourier integral

$$F(\tilde{\nu}) = \mathrm{i}\int_0^{\infty} \exp(\mathrm{i}\tilde{\nu}t)\, Z(t)\, \mathrm{d}t \qquad (1)$$

where $Z(t)$ is the complex correlator function that encodes the vibronic detail of the unperturbed spectrum. $Z(t)$ is obtained from the Fourier transform of the experimental, unperturbed spectrum. The effect of inhomogeneous van der Waals broadening on the spectrum, i.e., the consequence of a distribution of 1:1 absorber−perturbers at different interparticle separations, is accounted for by the convolution of $Z(t)$ with the pressure-dependent dipole correlator, $f_P(t)$, which contains the analytical forms of the absorber−perturber interaction potentials, viz.

$$f_P(t) = \exp(4\pi D\int_0^{\infty} \mathrm{d}r\, r^2 g_{12}(r)\{\exp[\mathrm{i}t\Delta V(r)] - 1\}) \qquad (2)$$

where D is the number density of perturbers, r is the absorber−perturber separation, $g_{12}(r)$ is the (radial) pairwise distribution function of perturbers around an absorber, and $\Delta V(r)$ represents the vertical separation between the upper and lower state absorber−perturber interaction potentials, i.e., $V_e(r) - V_g(r)$. The use of $\Delta V(r)$ in eq 2 indicates the acceptability of the Franck−Condon approximation in expressing the pressure perturbation effects on the absorption spectrum of the absorber.

This method assumes that the changes in the line shape of the absorption spectrum, i.e., shifting and asymmetric broadening, are brought about by the *differences* in the binding properties of the van der Waals complexes between the ground- and excited-state absorber and the perturber species. Furthermore, we will use the Lennard-Jones (LJ) potential to represent both $V_g(r)$ and $V_e(r)$, i.e.,

$$V_{g,e}(r) = 4\epsilon_{g,e}\left[\left(\frac{R_{g,e}}{r}\right)^{12} - \left(\frac{R_{g,e}}{r}\right)^{6}\right] \qquad (3)$$

where $\epsilon_{g,e}$ and $R_{g,e}$ are the well depths and the $V = 0$ crossing points characteristic of the ground- and excited-state potentials, respectively. The use of this centrosymmertic potential for a molecule such as ABCO, in which the N-atom "chromophore" is located at one bridgehead, may be justified on the basis of ab initio calculations of the (n_N,$3s_N$) Rydberg state.[14] These results indicate considerable delocalization of the excited electron over the bridgehead carbons, especially the three atoms directly bonded to N. Furthermore, it is not practical to employ an anisotropic model for the ABCO−X complexes.

Within the centrosymmetric framework of the model, we exploit a very useful approximation for expressing the absorber−perturber radial distribution function, namely the Boltzmann factor of the ground-state interaction energy. Thus

$$g_{12}(r) \simeq \exp[-V_g(r)/k_B T] \qquad (4)$$

This function, which may be expected to represent $g_{12}(r)$ adequately at low perturber number densities, provides the only *separate* representation of the $V_{g,e}(r)$ functions, i.e., $V_g(r)$, in the model. Furthermore the use of eq 4 implies that the system is in thermal equilibrium, which is, indeed, the case for these static-cell experiments.

The method is implemented by first obtaining the (complex) Fourier transform of the unperturbed spectrum, $Z(t)$. Next, the dipole correlator function, $f_P(t)$, is constructed from a model that contains the perturber number density, M, and the four-parameter $\Delta V_{g,e}(r)$ functions (see eq 3). Then the two functions are convolved with each other to produce another complex time domain function, $P(t)$, where

$$P(t) = Z(t)\cdot f_P(t) \qquad (5)$$

and finally, the calculated pressure-perturbed spectrum is obtained from the real part of the back-Fourier transform of $P(t)$, i.e.,

$$F_{calc}(\tilde{\nu}) = R\int_{-\infty}^{+\infty} \exp(\mathrm{i}\bar{\nu}t)\, P(t)\, \mathrm{d}t \qquad (6)$$

The residuals of the observed and calculated spectra are computed and then minimized with respect to the four fitting (LJ) parameters using a standard nonlinear regression algorithm. Although this method requires numerous Fourier transforms, it is reasonably efficient. Convergence is typically obtained after 100 or 200 iterations, which require only modest computational cost. Reduced χ^2 values are typically 10^{-5}−10^{-3}. Although it is theoretically possible to regress the data into the optimized four LJ parameters in the time domain (eqs 1, 2, and 5), it was much more effective to work in frequency space (eqs 1 and 6) despite the need to transform back to frequency after each iteration.

Another assumption that we have employed here is that pure collisional dephasing of the excited state is unimportant relative to van der Waals broadening. If collisional or interruption broadening were to be included in this model, it would enter through an additional factor incorporated into the dipole correlator. Thus, $Z(t)$ would be convolved with $f_P(t)$ and also $g_P(t)$, where

$$g_P(t) = \exp(-\Gamma t) \quad (7)$$

$$\Gamma = \pi R_{eff}^2 D(8k_B T/\pi\mu)^{1/2} \quad (8)$$

and πR_{eff}^2 is the effective collisional cross section between ABCO* and the perturber, D is the perturber number density, and μ is the reduced mass of the ABCO−perturber pair.

The effect of including $g_P(t)$ in the convolution of $Z(t)$ is to contribute a Lorentzian line shape to the perturbed spectrum. This homogeneous dephasing is not included in the present analysis because we assumed that collisional dephasing is unimportant relative to van der Waals broadening. This is justified on the basis of the relatively strong interaction between ABCO* and the perturbers studies here (see below). A similar justification was used for the noninclusion of collisional dephasing in the perturbation of the $\tilde{X} \rightarrow \tilde{A}$ transition in ammonia.[5]

Experimental Section

Some experiments were carried out at Northeastern University using a Varian 2300 spectrophotometer operating with a band-pass of 0.08 nm (ca. 20 cm^{-1}). At Indiana State University, measurements were performed on a Cary 5 spectrophotometer with a band-pass of 0.05 nm (ca. 13 cm^{-1}). Spectra were acquired on this instrument at a constant signal-to-noise ratio. In both cases, the spectrophotometer was purged with dry N_2 or Ar. The high-pressure cell was constructed from a stainless steel six-way cube (MDC Mfg. Co., CU-075-6) fitted with "Del-Seal" blank flanges. To accommodate the optical windows, flanges having $^1/_2$ in. clearings were used on opposite sides of the cube. Surprasil windows ($^7/_8$ in. diameter, $^1/_2$ in. thick) were attached to the cube sides and flanges with Viton gaskets. The path length of the cell was 3 cm. The perturber gas pressure was measured using a transducer (Omega Engineering Co., PX303-4KG10V) driven by a regulated power supply, and was converted to molarity using the Beattie-Bridgman equation of state (for He and Ar) and the van der Waals equation of state (for SF_6 and Xe). Calculations were performed on an IBM RS/2000 model 320 workstation using software based on standard spline, Fourier transform, and nonlinear regression programs.[17]

Results and Discussion

The static-cell absorption spectrum of vapor phase ABCO at 294 K is shown in Figure 1. Two electronic transitions, $S_0 \rightarrow S_1$ and $S_0 \rightarrow S_2$, are depicted, with origins at ca. 39 090 cm^{-1} and 43 100 cm^{-1}, respectively. In addition, Figure 1 shows the ABCO spectrum in *n*-hexane solution in which there is a complete loss of vibrational structure, as well as an overall blue shift in the Franck−Condon envelopes of the $S_0 \rightarrow S_1$ and $S_0 \rightarrow S_2$ transitions. In this study, we examined the perturbing effects of the rare gases Ar, He, Xe, and, in addition, SF_6, which is also chemically unreactive toward ABCO under the conditions studied here. One complication we faced in fitting the pressure-perturbed ABCO spectra stems from the distortion of the high-energy region of the $S_0 \rightarrow S_1$ transition caused by the tail of the more strongly allowed $S_0 \rightarrow S_2$ transition. This situation can be readily seen in Figure 1.

Perturbation by Ar. Figure 2 shows the $S_0 \rightarrow S_1$ transition of ABCO between ca. 39 000 and 42 500 cm^{-1} without perturber and in the presence of 2.35 M Ar (55.78 atm). In the latter case, it is clear that the vibronic features are asymmetrically broadened to the blue, while being shifted slightly to the red. Using the iterative Fourier reconvolution method described above, we were able to achieve very satisfactory fits to the perturbed spectrum in terms of the two pairs of LJ parameters (reduced χ^2 values of 10^{-4} are typical). Figure 2 also shows the optimized fit to this pressure-perturbed spectrum. We point out that the rising portion of the calculated spectrum below 39 000 cm^{-1} and the falling portion above ca. 42 300 cm^{-1} are due to the "wraparound effect", which is a computational property of the Fourier transform that forces the function to be continuous. In our fitting procedure we eliminated the importance of these two end regions by appropriately selecting the frequency range for the calculation of χ^2. The same arrangement was used in fitting the $S_0 \rightarrow S_2$ spectra. Because of the rising background (above ca. 40 500 cm^{-1}), due presumably to thermally assisted $S_0 \rightarrow S_2$ transitions, the LJ parameters obtained from the global fit to the $S_0 \rightarrow S_1$ spectrum are probably systematically biased. Indeed, the values of ϵ_g and R_g inverted from the $S_0 \rightarrow S_1$ spectrum are not in close agreement with those obtained from an analysis of the less encumbered $S_0 \rightarrow S_2$ transition. For example, the optimized values of the LJ parameters for the calculated pressure-perturbed

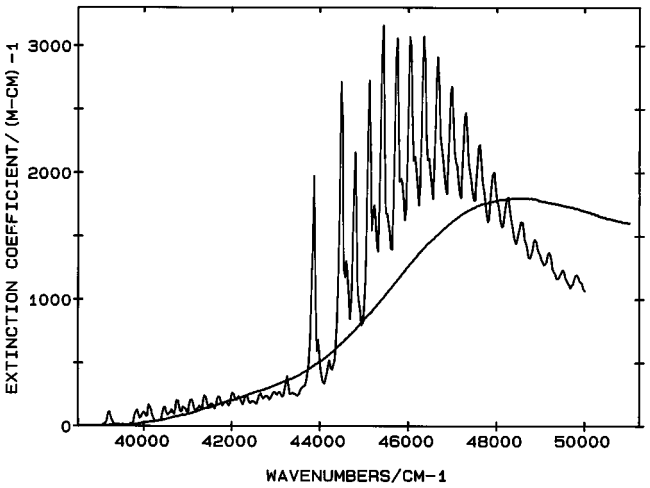

Figure 1. Electronic absorption spectra of ABCO in the vapor phase (structured) and in *n*-hexane solution (structureless) at 296 K. The origins of the $S_0 \rightarrow S_1$ and $S_0 \rightarrow S_2$ transitions are at 39 090 and 43 100 cm^{-1}, respectively.

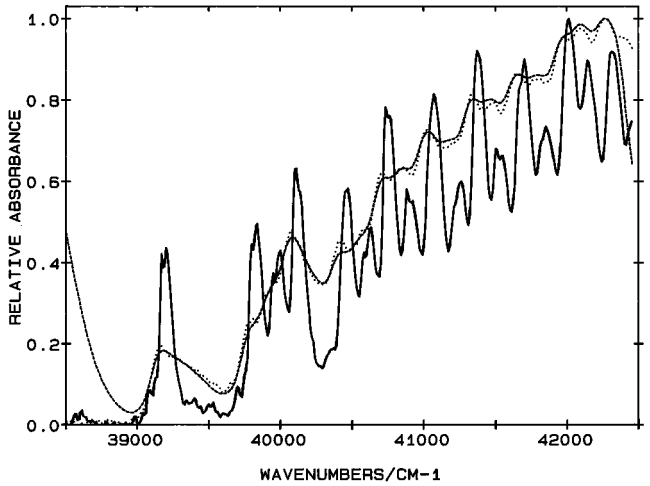

Figure 2. $S_0 \rightarrow S_1$ transition of ABCO vapor at 296 K: ABCO vapor only (—); in the presence of 55.78 atm (2.35 M) Ar (···); and the spectrum calculated from the iterative Fourier reconvolution method using Lennard-Jones potentials for the ground and excited states. The optimized parameters are cited in the text. The portions of the calculated spectrum below ca. 39 000 cm^{-1} and above ca. 42 000 cm^{-1} are caused by the "wraparound" effect, which is described in the text.

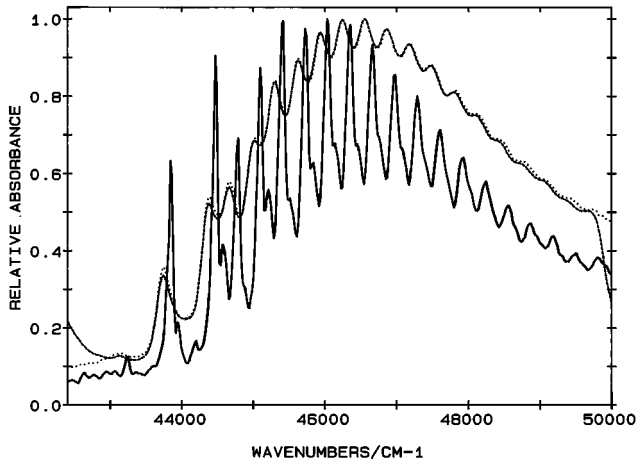

Figure 3. $S_0 \rightarrow S_2$ transition of ABCO vapor at 296 K: ABCO vapor only (—); in the presence of 55.78 atm (2.35 M) Ar (···); and the spectrum calculated from the iterative Fourier reconvolution method using Lennard-Jones potentials for the ground and excited states. The optimized parameters are listed in Table 1. The portions of the calculated spectrum below ca. 43 000 cm^{-1} and above ca. 49 700 cm^{-1} are caused by the "wraparound" effect, which is described in the text.

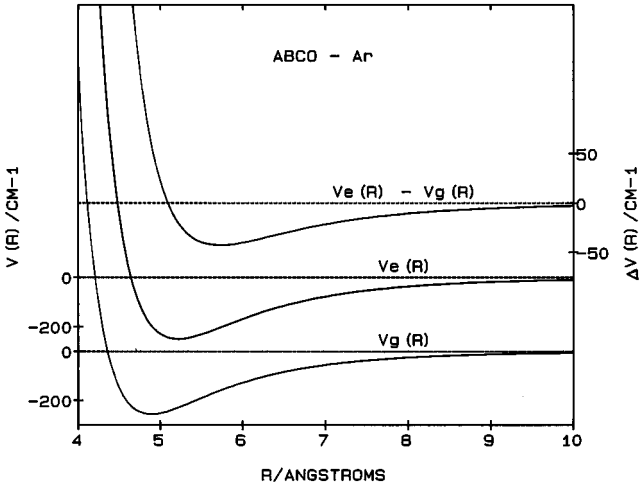

Figure 4. Plots of the optimized Lennard-Jones potentials $V_g(r)$ and $V_e(r)$ for the ABCO−Ar complex for the $S_0 \rightarrow S_2$ transition in ABCO. The parameters are listed in Table 1.

$S_0 \rightarrow S_1$ transition shown in Figure 2 are $R_{g,e} = 4.224$ and 4.400 Å, respectively, and $\epsilon_{g,e} = 366.6$ and 332.4 cm^{-1}, respectively. These values compare with $R_{g,e} = 4.357$ and 4.643 Å, respectively, and $\epsilon_{g,e} = 257.2$ and 250.7 cm^{-1}, respectively, obtained from an analysis of the $S_0 \rightarrow S_2$ transition for the same ABCO−Ar system.

Figure 3 shows the experimental unperturbed, Ar-perturbed, and the calculated Ar-perturbed spectra of ABCO for the $S_0 \rightarrow S_2$ transition under the same conditions as in Figure 1. Although there is no a priori basis at this point to favor one set of LJ parameters over the other vis-à-vis the analysis of the $S_0 \rightarrow S_1$ or the $S_0 \rightarrow S_2$ transitions, we will emphasize the results obtained from the latter transition in this discussion because of the concern mentioned earlier about the distortion of the $S_0 \rightarrow S_1$ transition and the question this raises about the reliability of the LJ parameters obtained from such data. In Figure 4, we present plots of the optimized LJ potentials obtained for the ABCO−Ar complex for the S_0 and S_2 states, as well as the difference potential, $\Delta V(r)$, pertinent to this transition.

It is instructive to consider these curves in order to obtain a qualitative understanding of how the iterative Fourier reconvolution predicts the effects of van der Waals broadening. At a given temperature and perturber number density there will be an ensemble of absorbers with a distribution of perturbers surrounding them according to the radial distribution given by eq 4. Suppose the mean absorber−perturber (center-to-center) distance is 7 Å. (This is the case for a well depth of ca. 300 cm^{-1} and a temperature of 300 K.) A vertical projection from the $V_g(r)$ curve at that point to $V_e(r)$ indicates that a given feature would be red-shifted by ca. 30 cm^{-1}. The actual distribution of states on the $V_g(r)$ surface projected onto the $V_e(r)$ surface gives the *line shape* of the shifted feature. Moreover, this red shift will increase as the perturber number density, i.e., its pressure, increases (r decreases), or as T decreases; see the ΔV curve in Figure 4. As the pressure increases further, there will be a point at which the spectral feature(s) will begin to blue shift (i.e., where $\Delta V > 0$). It should be mentioned that the concept of a "shift" in the maximum of a vibronic feature is not a definitive characterization of the effect of a perturber on the absorber spectrum. This is because there is substantial asymmetric broadening to the blue of a vibronic feature that accompanies the shifting of its maximum. Thus, perhaps a more meaningful quantitative characterization might be the shift of the centroid (first moment) of a vibronic feature relative to its unperturbed position.

Note that for the analysis of both transitions, $R_e > R_g$, which is expected because S_1 and S_2 have appreciable Rydberg character.[13,14] In the case of the $S_0 \rightarrow S_2$ transition, we see that ΔR, i.e., $R_e - R_g$, is 0.286 Å, which satisfactorily compares with a computed value of 0.30 obtained from a Monte Carlo integration of the S_0 and S_2 wave functions obtained from ab initio calculations.[18] It may seem surprising that ΔR is so small for Rydberg transitions, but this is also consistent with recent calculations that show considerable involvement of the C atoms in the excited-state wave functions.[14] The values of the LJ parameters obtained from the pressure perturbed $S_0 \rightarrow S_2$ transition of ABCO for Ar and the other perturbers studied, i.e., He, Xe, and SF_6, are listed in Table 1.

It is interesting to compare the binding energy of the ground-state ABCO−Ar van der Waals complex obtained from this analysis (i.e., 257 cm^{-1}) with empirical calculations recently reported by Shang et al.[11,12] On the basis of these calculations, these investigators suggested that three different 1:1 ABCO−Ar complexes exist representing geometries in which the Ar atom occupies different sites on the surface of the ABCO molecule. The binding energies of these complexes are estimated from these calculations to be 343, 276, and 241 cm^{-1}.[12] Under the static cell conditions at 296 K ($k_BT = 206$ cm^{-1}) pertinent to our studies, a distribution of ABCO−Ar complexes is expected to exist, and the well depth, ϵ_g, that we obtain from our pressure studies (i.e., 257 and 367 cm^{-1} based on the $S_0 \rightarrow S_2$ and $S_0 \rightarrow S_1$ transitions, respectively) represents a weighted average of these nonrigid ABCO−Ar complexes, and is reasonably consistent with the results of Shang et al.,[12] from which we obtain a weighted binding energy of ca. 300 cm^{-1} at 296 K.

We studied the effects of Ar perturbation of the ABCO spectra up to pressures of ca. 85 atm and found that the iterative Fourier reconvolution method provides reasonably consistent values of the four LJ parameters used to fit the perturbed spectra. For example, at 3.33 M (75.8 atm), the optimized $R_{g,e}$ and $\epsilon_{g,e}$ values for the $S_0 \rightarrow S_2$ transition are 4.422 and 4.671 Å and 264.4 and 254.2 cm^{-1}, respectively (cf. the values in Table 1). Over this pressure range we determined that the red shift of the 0−0 band of that transition was linear, with a shift coefficient of −1.45 cm^{-1}/atm, which compares with a value of −0.554 cm^{-1}/atm

TABLE 1: Lennard-Jones Parameters for the S_0 and S_2 States of ABCO and the Perturbers Studied at 296 K

perturber	P/atm	M	R_g/Å	ϵ_g/cm^{-1}	R_e/Å	ϵ_e/cm^{-1}	ΔR/Å	$\Delta\epsilon$/cm^{-1}	χ^2 [a]
He	69.32	2.74	5.227	113.9	5.685	79.7	0.458	−34.2	1.6×10^{-4}
Ar	55.78	2.35	4.357	257.2	4.643	250.7	0.286	−6.5	3.6×10^{-5}
Xe	14.60	0.652	4.940	592.9	4.984	644.2	0.044	51.3	2.3×10^{-4}
SF_6	11.20	0.532	5.224	341.0	5.373	415.4	0.149	74.4	2.6×10^{-4}

[a] Mean reduced χ^2 value for the fit.

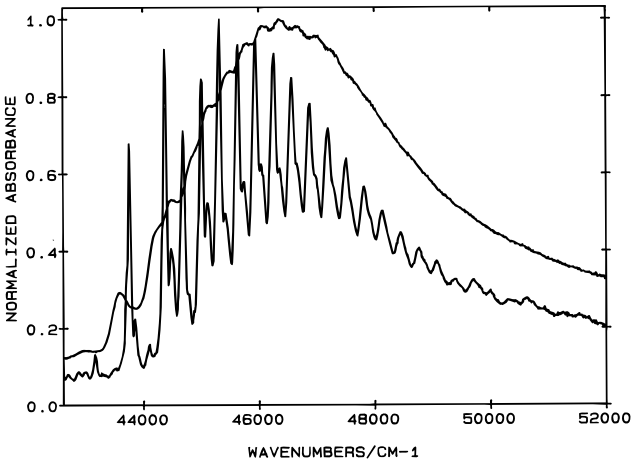

Figure 5. $S_0 \rightarrow S_2$ transition of ABCO vapor at 296 K alone and in the presence of 135 atm (5.75 M) Ar.

TABLE 2: Linear Shift Coefficients of the 0−0 Bands for the $S_0 \rightarrow S_1$ and $S_0 \rightarrow S_2$ Transitions of ABCO for Different Perturber Gases

perturber	$S_0 \rightarrow S_1$ (cm^{-1}/atm)	$S_0 \rightarrow S_2$ (cm^{-1}/atm)	press. range/atm
He	+0.997	+0.417	0−80
Ar	−0.554	−1.45	0−85
Xe	−4.10	−6.20	0−15
SF_6	−3.85	−5.23	0−22

for the $S_0 \rightarrow S_1$ transition. The larger susceptibility to Ar perturbation of the transition to the S_2 state is presumably a result of its larger cross section (and polarizability) vis-à-vis the S_1 state. The linear shift coefficients of the 0−0 bands of the ABCO $S_0 \rightarrow S_1$ and $S_0 \rightarrow S_2$ transitions for the perturbers studied here are summarized in Table 2. We see that for all the red-shifting perturbers (i.e., Ar, Xe, and SF_6), the shift coefficients are larger for the $S_0 \rightarrow S_2$ transition vis-à-vis the $S_0 \rightarrow S_1$ transition. The opposite situation is observed for He, a blue-shifting perturber, in which the shift coefficient is larger for $S_0 \rightarrow S_1$ transition than for $S_0 \rightarrow S_2$.

It is rather interesting to note that although the red shift of the 0−0 band is approximately linear with increasing Ar pressure, the Franck−Condon maximum of the vibronic features shifts to the blue. This behavior is evident in Figure 5, which shows how the $S_0 \rightarrow S_2$ transition is perturbed in the presence of 5.75 M (135 atm) of argon. To check the consistency of the four LJ potential parameters for the ABCO−Ar system, we computed pressure perturbed spectra by convolving the Fourier transform of the $S_0 \rightarrow S_2$ transition with the dipole correlator function (eq 2). In the latter function, we used the optimized values of R_g, ϵ_g, R_e, and ϵ_e, obtained from an analysis in which Ar is 2.35 M (55.78 atm) (see Table 1), and arbitrarily chosen values of D between 0 and 4 M (i.e., up to 80 atm; 0 M reproduces the unperturbed spectrum). The shifts of the 0−0 bands of the calculated transitions were plotted vs perturber pressure and found to be linear with a slope of −1.82 cm^{-1}/atm, which is in reasonable agreement with the experimentally observed value of −1.45 cm^{-1}/atm (see Table 2).

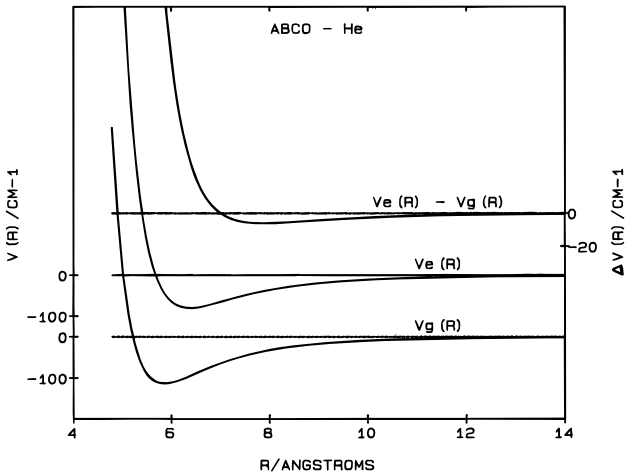

Figure 6. Plots of the optimized Lennard-Jones potentials $V_g(r)$ and $V_e(r)$ for the ABCO−He complex for the $S_0 \rightarrow S_2$ transition in ABCO. The parameters are listed in Table 1.

Perturbation by He. In the presence of He as a perturber, the ABCO spectra are blue-shifted. This behavior was also observed in the perturbation of such absorbers as CH_3I, NH_3, and acetone. The blue-shifting effect of He on the 0−0 band of the $S_0 \rightarrow S_2$ transition in ABCO is relatively small; the linear shift coefficient is +0.417 cm^{-1}/atm (see Table 2). As mentioned above, this is less than twice the effect relative to the $S_0 \rightarrow S_1$ transition.

We note that in previous studies using He as a perturber, i.e., with the absorbers CH_3I, NH_3, and acetone, the excited-state interaction potentials had to be modeled using *repulsive* potentials. Furthermore, the ground-state interaction potentials were either unbound or very weakly bound. In the case of ABCO, however, we find that the ground-state potential obtained from the iterative Fourier reconvolution method indicates that the ground-state He complex is considerably bound (e.g., $\epsilon_g \simeq$ 114 cm^{-1}). Perhaps for this reason, we find that the excited-state potential (for the ABCO S_2 state) is also nonrepulsive, although it is less bound than the ground-state complex, ($\epsilon_e \simeq$ 80 cm^{-1}, see Table 1). These potentials, along with $\Delta V(r)$, are shown in Figure 6.

It may seem at first surprising that both the S_1 and S_2 transitions in ABCO are blue-shifted by He despite the fact that the interaction potentials for both states are bound, but an examination of the $\Delta V(r)$ curve shows that this curve is much more shallow than that for the ABCO−Ar complex. As mentioned in the discussion of the ABCO−Ar system above, the effect of a perturber is both to broaden a vibronic feature asymmetrically to the blue and to red shift the maximum. In the case of He, where the $\Delta V(r)$ curve is more shallow than that for Ar—and the zero-crossing point is located at a larger r value (lower pressure)—it appears that the overall effect is to cause the vibronic features to undergo a net small blue shift in their maxima. Thus, it is the overall *shape* of the $\Delta V(r)$ curve that encodes the information about the direction of the shift for a particular perturber at a certain number density, i.e., the distribution of states along the $V_g(r)$ potential.

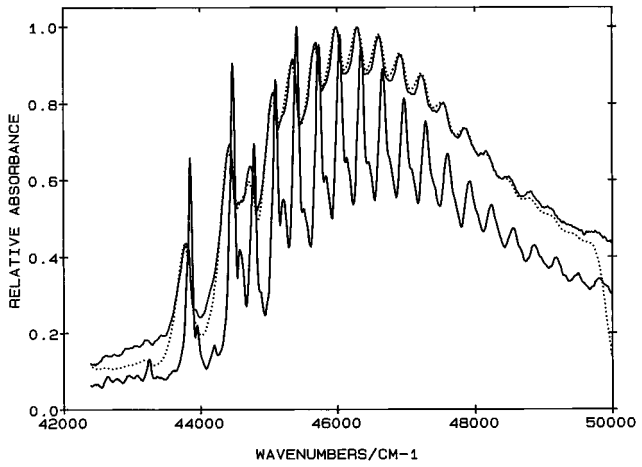

Figure 7. $S_0 \rightarrow S_2$ transition of ABCO vapor at 296 K: ABCO vapor only (—); in the presence of 11.2 atm (0.532 M) SF_6 (···); and the spectrum calculated from the iterative Fourier reconvolution method using Lennard-Jones potentials for the ground and excited states. The optimized parameters are listed in Table 1.

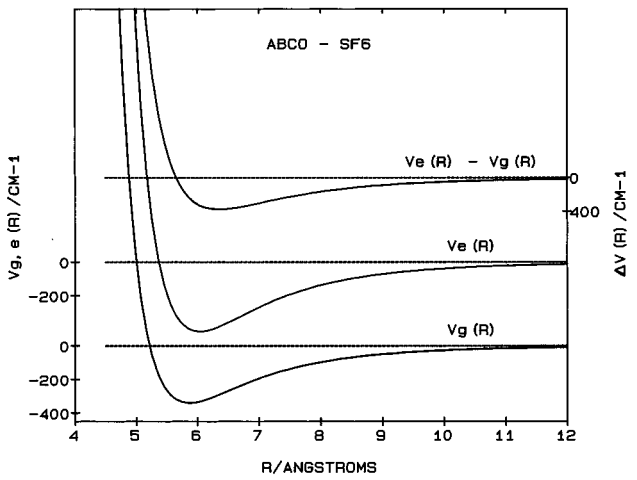

Figure 8. Plots of the optimized Lennard-Jones potentials $V_g(r)$ and $V_e(r)$ for the ABCO−SF_6 complex for the $S_0 \rightarrow S_2$ transition in ABCO. The parameters are listed in Table 1.

Perturbation by SF_6 and Xe. We examined the effects of SF_6 and Xe, both nonpolar and polarizable perturbers having relatively large collision diameters (ca. 5.20 and 4.05 Å, respectively)[19] on the ABCO spectra. In the case of SF_6, one is limited by its vapor pressure at 296 K (22.8 atm, ca. 1.32 M), although because of the large perturbation cross section of SF_6 we did not exceed 15 atm. As in the case of Ar, perturbation by SF_6 and Xe induce red shifts in the $S_0 \rightarrow S_1$ and $S_0 \rightarrow S_2$ transitions, and the vibronic features are asymmetrically broadened to the blue. The $S_0 \rightarrow S_2$ ABCO transition perturbed by 0.532 M (11.2 atm) of SF_6 is shown in Figure 7.

Both SF_6 and Xe are more potent perturbers of the ABCO transitions than Ar, as evidenced by their much larger linear shift coefficients (see Table 2). Consistent with these data, we see that the ground-state well depths, ϵ_g, are larger than that for the ABCO−Ar complex, e.g., 592.9, 341.0, and 257.2 cm^{-1} for Xe, SF_6, and Ar, respectively. It is also interesting that for SF_6 and Xe the excited-state ABCO(S_2)−Ar well depths are larger than those for the ground-state complex, i.e., by about 74 and 51 cm^{-1} for SF_6 and Xe, respectively. This trend is different relative to SF_6 perturbation of the $\tilde{X} \rightarrow \tilde{B}$ (5p,6s) transition in CH_3I in which $\epsilon_g - \epsilon_e$ (but for which $R_e > R_g$).[4] Figure 8 shows the Lennard-Jones potentials for the ABCO−SF_6 system, as well as $\Delta V(r)$.

In the case of the ABCO−SF_6 system, we have reported previously that SF_6 quenches the $S_1 \rightarrow S_0$ fluorescence of ABCO with very high efficiency.[15] In this case linear Stern−Volmer kinetics is followed (up to the maximum pressure studied, ca. 10 Torr) with a second-order quenching rate constant of 5.4×10^{11} M^{-1} s^{-1}, which is on the order of the gas kinetic collision frequency. Interestingly, we observed a leveling off in the fluorescence lifetime (and quantum efficiency) of ABCO(S_1) in the case of Xe perturbation, which is similar to the situation for Ar (and He) perturbation. With Xe, for example, the ABCO-(S_1) fluorescence quantum efficiency falls to about 35% of the zero-pressure value at a Xe pressure of only about 100 Torr and remains constant at that level up to 1 atm. The fluorescence lifetime undergoes a concomitant decrease and leveling off in this pressure range, although the extent of the decrease in this case is larger, ca. 78%, indicating an increase in the radiative rate constant. These differences in the photophysical consequences of collisions between ABCO(S_1) and SF_6 and Xe have been interpreted in terms of the higher electron affinity of SF_6.[15] In this context it is noteworthy that in alkane solution perfluorinated saturated hydrocarbons quench saturated tertiary amine fluorescence at the diffusion-controlled rate.[20]

The effects of rare gas (and SF_6) perturbation on the photophysical properties of ABCO(S_1) have been interpreted previously in terms of a reversible complex formed between ABCO(S_1) and the perturber.[15] As noted above, it seems evident that the formation of the ABCO(S_1)−SF_6 complex leads to nonradiative decay. For the rare gases, the dissociation rate constants of the ABCO(S_1)−rare gas complexes have been estimated at 296 K.[15] For complexes with perturbers He, Ar, and Xe, the rate constants reported are in the ratio 3.9:1.6:1.0, respectively. This trend qualitatively parallels the well depths of the ABCO(S_1)−rare gas complexes, ϵ_e (see Table 1). To estimate the dissociation rate constants of these complexes from well depths, one would need to know the interparticle vibrational eigenvalues in order to employ a suitable reaction rate model.

Other Studies of the ABCO−Ar System. In their study of the mass-resolved excitation spectra of ABCO in a supersonic jet expansion with Ar, Shang et al.[11,12] reported three features associated with the mass number of the ABCO−Ar complex. Two of these features are sharp and are shifted to the red and blue relative to the 0−0 transition of the bare ABCO molecule by 28 and 47 cm^{-1}, respectively. The third feature is broad and appears at ca. 245 cm^{-1} to the blue of the ABCO origin. These features are interpreted as 0−0 transitions associated with the three different 1:1 ABCO−Ar cluster geometries mentioned above). Shang et al. deduce the qualitative shapes of the interparticle potentials associated with the S_0 and S_1 states of the three ABCO−Ar complexes. These pairs of potentials differ from each other with respect to the relative positions of the minima as well as their well depths.

It is interesting to compare the potentials for the ABCO−Ar complex(es) deduced by Shang et al. with those obtained in this study. There are fundamental differences in the experimental conditions used by Shang et al. and by us in obtaining this information. The pair potentials that we obtain in this study are based on a model that assumes that a *statistical distribution* of Ar atoms surrounds an ABCO molecule at thermal equilibrium at 296 K. In fact, this assumption is explicitly represented by our use of the Boltzmann factor of the interaction potential of the ABCO(S_0)−Ar complex [$V_g(r)$] as the radial distribution function of these complexes (eqs 3 and 4). Furthermore, this one-dimensional potential is a statistically weighted average of

such 1:1 complexes (having, of course, different geometries) mapped onto a centrosymmetric space. In addition, the number density of Ar atoms determines the radial population profile of Ar atoms with respect to the ABCO absorber on the $V_g(r)$ potential surface (eq 2). Because the $V_{g,e}(r)$ potentials are inverted from the experimentally observed pressure-perturbed spectra obtained under thermal equilibrium conditions, it follows that the potentials thus obtained are, perforce, consistent with the shift and line shape change observed for these perturbed spectra.

The conditions that apply to the experiments of Shang et al. are quite different. In the situation of a jet-cooled beam (ca. 10 K), discrete 1:1 ABCO−Ar complexes (and also higher order complexes) are formed. The mass-resolved spectra that are observed for these different complexes give information about the specific 0−0 transition energy shifts of these complexes relative to the uncomplexed absorber.

The differences between the jet-cooled beam and the static cell, room-temperature experiments reported here can be clarified by examining the potential energy plots shown in Figure 4. In our experiments, in which we observe a red shift in the maximum of the 0−0 band, transitions originate from the region of the $V_g(r)$ surface in which r is fairly large (ca. 7 Å), whereas in the jet-cooled work of Shang et al., transitions presumably originate from the bottom of the well (ca. 4.8 Å) (ignoring zero-point effects). From Figure 4, vertical projections from these $V(r)$ positions onto the $\Delta V(r)$ curve indicate red and blue shifts of ca. 20 and 80 cm^{-1}, respectively. On the basis of the 0−0 shifts and the computational results reported by Shang et al., we calculate a weighted-average origin (blue) shift (taking into account the number of sites on ABCO at which the Ar atom is suggested to bind) of ca. +72 cm^{-1}, which compares with the value of +80 cm^{-1} that we find from our centrosymmetric potentials.

Acknowledgment. We express our gratitude to Dr. S. L. Frye and Mr. E. Reid for implementing some of the code used in the iterative Fourier reconvolution analysis.

References and Notes

(1) (a) Robin, M. B.; Kuebler, N. A. *J. Mol. Spectrosc.* **1970**, *33*, 274. (b) Miladi, M.; Falher, J.-P.; Roncin, J.-Y. *J. Mol. Spectrosc.* **1975**, *55*, 81. (c) Robin, M. B. *Higher Excited States of Polyatomic Molecules*; Academic Press: New York, 1974; Vol. 1, pp 8−47.

(2) (a) Altenloh, D. D.; Russell, B. R. *J. Phys. Chem.* **1982**, *86*, 1960. (b) Altenloh, D. D.; Ashworth, L. R.; Russell, B. R. *J. Phys. Chem.* **1983**, *87*, 4348.

(3) Halpern, A. M.; Ziegler, L. D. *Chem. Phys. Lett.* **1989**, *161*, 1.

(4) Halpern, A. M. *J. Phys. Chem.* **1992**, *96*, 2448.

(5) Halpern, A. M.; Ramachandran, B. R. *J. Phys. Chem.* **1993**, *97*, 77.

(6) Halpern, A. M.; Ramachandran, B. R. *J. Chem. Phys.* **1993**, *98*, 8593.

(7) (a) Halpern, A. M.; Roebber, J. L.; Weiss, K. *J. Chem. Phys.* **1968**, *49*, 1348. (b) McKinney, T. M. *Spectrochim. Acta, Part A* **1969**, *42*, 501.

(8) (a) Parker, D. H.; Avouris, P. *Chem. Phys. Lett.* **1978**, *53*, 151. (b) Gonohe, H.; Yatsuda, N.; Mikami, N.; Ito, M. *Bull. Chem. Soc. Jpn.* **1982**, *55*, 2796. (c) Fujii, M.; Mikami, N.; Ito, M. *Chem. Phys.* **1985**, *99*, 193.

(9) Halpern, A. M.; Gerrity, D. P.; Rothberg, L. J.; Vaida, V. *J. Chem. Phys.* **1982**, *76*, 102.

(10) Halpern, A. M. *J. Am. Chem. Soc.* **1974**, *96*, 4392.

(11) Shang, Q. Y.; Moreno, P. O.; Li, S.; Bernstein, E. R. *J. Chem. Phys.* **1993**, *98*, 1876.

(12) Shang, Q. Y.; Moreno, P. O.; Dion, C.; Bernstein, E. R. *J. Chem. Phys.* **1993**, *98*, 6769.

(13) Galasso, V. *Chem. Phys.* **1997**, *215*, 183.

(14) Disselkamp, R.; Shang, Q.-Y.; Bernstein, E. R. *J. Phys. Chem.* **1995**, *99*, 7227.

(15) Halpern, A. M.; Taaghol, A. *J. Phys. Chem.* **1989**, *93*, 144.

(16) (a) Page, J. B.; Tonks, D. L. *J. Chem. Phys.* **1981**, *75*, 5694. (b) Chen, C. K.; Page, J. B. *Chem. Phys. Lett.* **1984**, *104*, 609. (c) Chen, C. K.; Page, J. B. *J. Chem. Phys.* **1983**, *77*, 5234.

(17) Press, W. H.; Flannery, B. P.; Teukolsky, S. A.; Vetterling, W. T. *Numerical Recipes*; Cambridge University Press: Cambridge, 1986; pp 86−89, 386−397, 521−529.

(18) Halpern, A. M. *J. Mol. Spectrosc.* **1996**, *180*, 154.

(19) (a) Halpern, A. M.; Wryzykowska, K. *J. Photochem.* **1981**, *15*, 147. (b) Alford, P. C.; Cureton, C. G.; Lampert, R. A.; Phillips, D. *Chem. Phys. Lett.* **1978**, *55*, 100.